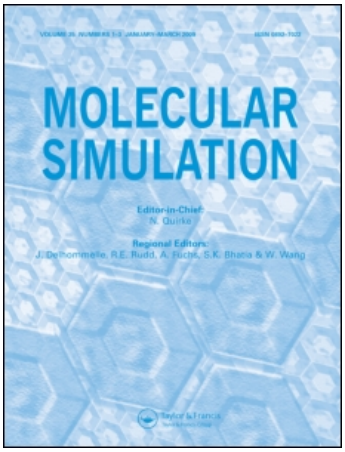

Molecular Simulation
Publication details, including instructions for authors and subscription information:
http://www.informaworld.com/smpp/title~content=t713644482

Molecular simulations of adsorption and diffusion of RDX in IRMOF-1

Ruichang Xiong[a]; Jared T. Fern[a]; David J. Keffer[a]; Miguel Fuentes-Cabrera[b]; Donald M. Nicholson[c]
[a] Department of Chemical and Biomolecular Engineering, University of Tennessee, Knoxville, TN, USA [b] Oak Ridge National Laboratory, Joint Institute for Computational Science, University of Tennessee and Center for Nanophase Materials Sciences, Oak Ridge, TN, USA [c] Computer Science and Mathematics Division, Oak Ridge National Laboratory, Oak Ridge, TN, USA

To cite this Article Xiong, Ruichang , Fern, Jared T. , Keffer, David J. , Fuentes-Cabrera, Miguel and Nicholson, Donald M.(2009) 'Molecular simulations of adsorption and diffusion of RDX in IRMOF-1', Molecular Simulation, 35: 10, 910 — 919
To link to this Article: DOI: 10.1080/08927020902818013
URL: http://dx.doi.org/10.1080/08927020902818013

Molecular Simulation
Vol. 35, Nos. 10–11, September 2009, 910–919

Taylor & Francis
Taylor & Francis Group

Molecular simulations of adsorption and diffusion of RDX in IRMOF-1

Ruichang Xiong[a], Jared T. Fern[a], David J. Keffer[a]*, Miguel Fuentes-Cabrera[b] and Donald M. Nicholson[c]

[a]*Department of Chemical and Biomolecular Engineering, University of Tennessee, Knoxville, TN 37996, USA;* [b]*Oak Ridge National Laboratory, Joint Institute for Computational Science, University of Tennessee and Center for Nanophase Materials Sciences, Oak Ridge, TN, USA;* [c]*Computer Science and Mathematics Division, Oak Ridge National Laboratory, Oak Ridge, TN, USA*

(*Received 25 November 2008; final version received 6 February 2009*)

In order to test the feasibility of using metal-organic frameworks (MOFs) to pre-concentrate explosive molecules for detection, molecular simulations of hexahydro-1,3,5-trinitro-1,3,5-triazine (RDX) within IRMOF-1 were performed. Grand canonical Monte Carlo (GCMC) simulations were used to generate adsorption isotherms for pure RDX, RDX in dry air, and RDX in wet air. In addition to the isotherms, the GCMC simulations provide adsorption energies and density distributions of the adsorbates within the MOF. Molecular dynamics simulations calculate diffusivities and provide a detailed understanding of the change in conformation of the RDX molecule upon adsorption. The presence of dry air has little influence on the amount of RDX that adsorbs. The presence of wet air increases the amount of RDX that adsorbs due to favourable interactions between RDX and water. We found a Henry's law constant of 21.2 mol/kg/bar for both pure RDX and RDX in dry air. The RDX adsorption sites are located (i) in big cages, (ii) near a vertex, and (iii) between benzene rings. The energy of adsorption of RDX at infinite dilution was found to be -9.2 kcal/mol. The distributions of bond lengths, bond angles and torsion angles in RDX are uniformly slightly broader in the gas phase than in the adsorbed phase, but not markedly so. The self-diffusivity of RDX in IRMOF-1 is a strong function of temperature, with an activation energy of 6.0 kcal/mol.

Keywords: metal-organic framework; RDX; adsorption; diffusion; molecular simulation

1. Introduction

There are many technologies for the detection of explosive molecules [1,2], including mass spectroscopy, ion mobility, surface acoustic wave spectroscopy, Swager-lasing-polymers, and MEMs devices. These detection devices incorporate some level of sampling and pre-concentration. Unfortunately, current preconcentrators do not trap explosives specifically.

Metal-organic frameworks (MOFs) are a class of nanoporous adsorbents, which hold promise for preconcentration of explosive molecules. MOFs are composed of two distinct structural units, the metal connector and the organic linker, shown in Figure 1, which represents the specific example of IRMOF-1. Changing the connector and linker allows creation of MOFs that share similar structures but have pores with different sizes, shapes, and chemical functionalities [3]. That the size, shape, and chemical functionality of the pores can be modified readily has made MOFs a strong candidate for the storage of hydrogen [4–6] and methane [3,7]. A similar concept can be applied to tailor the explosive selectivity and storage capabilities of MOFs. Fuentes-Cabrera et al. [8] proposed MOFs as preconcentrator materials because of their unique measured and calculated properties. Recently, it has been reported by Ni et al. [9] that MOFs have successfully preconcentrated Dimethyl methylphosphonate (DMMP). This demonstrates that MOFs can be quite useful as a selective preconcentrator, however, there are no published reports of the use of MOFs in preconcentrators for explosive compounds.

In this paper, molecular simulation has been performed to investigate the capability of IRMOF-1 [3] as an adsorbent for explosive preconcentration. Specifically, we study the explosive hexahydro-1,3,5-trinitro-1,3,5-triazine (RDX, CAS # 121-82-4), as shown in Figure 2. RDX is an important energetic material, and is widely used as rocket propellant and explosive. For example, RDX is used as a component of the plastic explosive C-4.

Classical force field-based molecular dynamics (MD) has proven to be a valuable tool in the study of RDX [10,11] in the bulk phase. A number of properties of RDX, such as vibrational frequencies and lattice binding energy and dimensions, can be reproduced in satisfactory agreement with experimental data [11].

In this work we examine RDX adsorption in IRMOF-1. The structure of IRMOF-1 is shown in Figure 1. IRMOF-1 has been studied as a starting point for a number of theoretical investigations on adsorption, for example, the storage of hydrogen [12]. IRMOF-1 contains two types of cages, which we will denote as 'big' and 'small'. The dimensions of the two types of cages are the same; both are cubic with a length of 12.92 Å [3]. However, the accessible volume in the two types of cages is different due to the orientation of the benzene rings. Big cages with a size of

*Corresponding author. Email: dkeffer@utk.edu

ISSN 0892-7022 print/ISSN 1029-0435 online

DOI: 10.1080/08927020902818013
http://www.informaworld.com

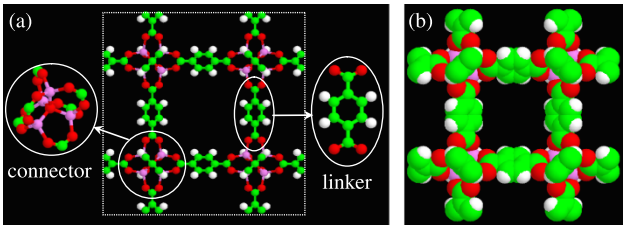

Figure 1. (a) IRMOF-1 structure with a small cage in the centre; (b) space-filling image of IRMOF-1 (violet, Zn; red, O; green, C; white, H).

14.3 Å in diameter consist of benzene rings in which the benzene planes are normal to a vector pointing to the centre of the cell and small cages with a size of 10.9 Å in diameter consist of benzene rings in which the benzene planes are oriented towards the centre of the cell [13]. The adsorption sites in big and small cages are not equivalent [14]. Figure 1(a) and (b) show a unit cell, containing eight cages, with a small cage at the centre of the image. The space filling image in Figure 1(b) gives both an indication of the accessible pore volume as well as a view of the orientation of the benzene rings. All six faces of the small cage open up to big cages and *vice versa*.

In this work, classical grand canonical Monte Carlo (GCMC) simulations were used to investigate the capability of IRMOF-1 to adsorb RDX. We are only interested in room temperature (300 K) and low partial pressure (< 1 bar) since these are the typical conditions under which explosives detection occurs. (The purpose of preconcentrators is to concentrate material that may be present only in parts per billion (ppb) or parts per trillion levels (ppt) in air. For example, equilibrium vapour pressure of RDX at room temperature is 6 ppt [15].) Classical force field-based MD simulations were used to calculate the self-diffusivity of RDX in IRMOF-1. The GCMC simulations were first performed for pure RDX in order to establish a baseline. Simulations for adsorption of RDX from dry air (N_2 and O_2) and wet air (including H_2O) were also performed to understand the competitive adsorption.

2. Interaction potential

For any classical force field-based molecular simulation, it is essential and important to choose an appropriate interaction potential as an input to the simulation. For the explosive adsorbate molecule, RDX, a number of intramolecular force fields have been proposed. Wallis and Thompson [10] constructed a new potential energy surface for MD simulation to study conformational changes of RDX in isolation and in a dense Xe gas. Chambers and Thompson [16] further refined this potential

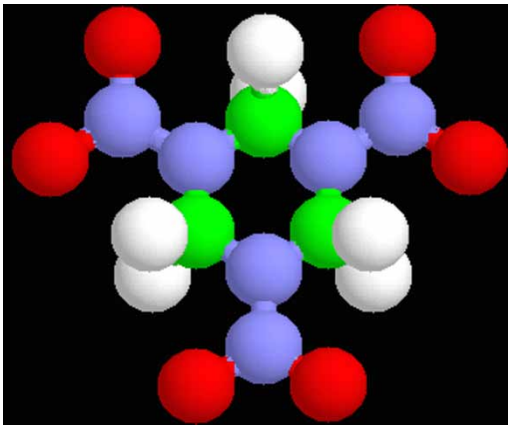

Figure 2. RDX structure (blue, N; red, O; green, C; white, H).

energy surface. Boyd et al. [11] generated an empirical non-reactive force field for RDX.

In this work, we employ a non-reactive, fully flexible, atomistic interaction potential for RDX that takes features from both Wallis and Thompson as well as Boyd et al. [10,11]. Essentially, we use all of the features of the potential from Boyd et al. except the non-Coulombic contribution to the non-bonded intramolecular and intermolecular interactions. The non-Coulombic non-bonded interactions are taken from Wallis and Thompson, who used a Lennard-Jones (LJ) form. This allows us to maintain a common form of the dispersive interaction potential with the other species – N_2, O_2 and H_2O – that are also present in the simulation. The RDX intramolecular force field includes bond stretching, angle bending, torsion and non-bonded interactions. The electrostatic interaction is due to a permanent charge distribution, modelled as point charges at each atom centre.

The simulations in dry air include molecular nitrogen and oxygen. It has long been known that it is important to include the effect of the quadrupole moment in the adsorption of N_2 [17]. Therefore, we used a potential that includes quadrupoles for both N_2 and O_2. We used the three-site TraPPE force field, which is an optimised potential for vapour–liquid equilibria calculations [18,19]. This has also been used by Yang et al. [20] who successfully simulated N_2, O_2 and its mixture with CO_2 in Cu-BTC MOF. In this potential, each atom of the molecule is modelled by a LJ site on which a negative point charge is placed. To maintain charge neutrality, a positive point charge is placed at the centre-of-mass (COM) of the molecule. In the published TraPPE force field, bond stretching is neglected. We added bond stretching to N_2 and O_2 with a harmonic potential [21,22].

The simulations of wet air include water. There are many choices for water potential. In this work, we use a three-site model [23]. The most commonly used three-site models are the transferable intermolecular potential with

three interaction sites (TIP3P) [24], the simple point-charge (SPC) model [25] and their variants. Greathouse and Allendorf [26] used the flexible SPC model [27] to simulate water interacting with IRMOF-1. In this work, we employed a flexible 3-site TIP3P potential [28], which also maintains a similar level of description in all adsorbate molecules. The H_2O molecule is modelled by an LJ site on the oxygen and a positive charge placed on each hydrogen atom and negative double charge placed on the oxygen atom to maintain charge neutrality.

There is an understanding that the use of water models parameterised to bulk data in nanoporous systems has a systematic error associated with it. For example, simulations of water in the silicalite zeolites [29] or in Cu-BTC MOF [30], require some empirical adjustment to match experiment. This limitation in potential is addressed later on.

We have several choices for the treatment of the MOF. The first choice involves the mobility of framework atoms. Simulations have been performed comparing the adsorption isotherms of hydrogen in flexible and rigid IRMOF-1. There is a body of work describing the effect of a rigid lattice on the mobility of adsorbates in crystalline nanoporous materials. This work shows that for small adsorbates, the effect of frame rigidity is nominal [31–34]. However, for larger adsorbates, the effect may be significant [35,36].

Studies of MOFs indicate that framework flexibility may be more important in MOFs than in zeolites and other nanoporous materials [37]. Nevertheless, in this work we have assumed a rigid framework, as has been used in other simulations of adsorption in MOFs [7,12,13,30,38–40]. This choice is also motivated by the fact that there are many more framework atoms than adsorbate atoms at low loadings, thus the computational effort is reduced by two or more orders of magnitude by using a rigid framework. In this case, the coordinates of the framework IRMOF-1 are set at their equilibrium coordinates as determined via experimental X-ray diffraction [3].

There are several potentials that can be used for IRMOF-1, such as universal force field [41], DREIDING force field [42], and OPLS force field [43]. Greathouse and Allendorf [26] used the CVFF force field for structurally flexible IRMOF-1 to do MD simulation for H_2O adsorption. Later Greathouse and Allendorf [44] provided a detailed validation for this force field to demonstrate that it can predict a number of important properties of MOFs accurately. Tafipolsky et al. [45] developed an *ab initio* parameterised MM3 force field, which is a fully bonded but flexible force field that can predict IRMOF-1 structure successfully. Here, we employed the MM3 force field from Tafipolsky et al. in which the LJ parameters are taken from Allinger et al. [46,47], which is the same source for LJ parameters used for RDX. We acknowledge that Tafipolsky et al. have indicated that, in their determination of the partial charge of atoms, there is uncertainty on some charges (especially the central oxygen atom). These charges may have a non-negligible impact in the calculation of thermodynamic properties such as adsorption isotherms.

For all intermolecular interactions, the mixture parameters were determined via Lorenz–Berthelot mixing rules [48]. The electrostatic interactions were handled using the spherically truncated charge-neutralised procedure of Wolf et al. [49]. The LJ potential and electrostatic potential were truncated at 18 Å. Potential parameters for all the adsorbates and framework can be found in the cited literature and part of them are listed in the supporting information. Due to the relatively long cut-off distance, no long-range corrections were applied for LJ interaction, as has been done previously [40]. Standard periodic boundary conditions and the minimum image convention were employed in all three dimensions.

3. Simulation methods

Classical equilibrium MD simulations were performed to obtain configurations and diffusivities of RDX adsorbed in nanoporous materials. We integrated the equations of motion using the two-time step r-RESPA algorithm of Tuckerman et al. [50]. Intramolecular degrees of freedom were accounted for in the short time loop, with a step size of 0.2 fs. There were 10 short steps per long time step. The temperature was controlled using the Nosé–Hoover thermostat [51,52]. We equilibrated the system for 2 ns. Following equilibration, we simulated an additional 8 ns for data collection. During data production, positions of the COM of the RDX molecules were saved every 5 ps and were used to calculate the self-diffusivity via the Einstein relation. Uncertainties in the self-diffusivity are reported as the standard deviation (SD) of the x, y, and z components of the diffusivity.

Also in this work, conventional GCMC simulations were performed to obtain adsorption isotherms, which relate the loading (i.e. the weight fraction of adsorbate in the adsorbate/adsorbent system) to the bulk pressure of the adsorbate gas in equilibrium with the adsorbent. The GCMC simulation technique for molecular systems is from Wang et al. [53]. We performed GCMC simulation with four types of moves: (1) molecular translation based on COM, (2) molecular rotation based on COM, (3) molecular insertion with random position and random orientation, (4) molecular deletion of a molecule in the system. Translation and rotation are accepted or rejected according to Metropolis procedure [54] based on $e^{-\beta\Delta H}$, where ΔH is the change in the total energy as a result of the move. The acceptance ratio is adjusted to 50% based on the maximum size of position changes or rotational angle changes. The inserted particle was chosen by randomly picking a configuration from the

pool, where a large number of ideal gas equilibrium configurations at specified temperature are stored.

We will show below, using MD simulation, that there is no significant difference in the distribution of the intramolecular conformations of RDX in bulk gas phase and in the adsorbed phase at the low loadings of interest. Therefore, intramolecular relaxation of the RDX was not sampled in the GCMC simulations, increasing the computational efficiency of the GCMC simulations.

Each of the GCMC moves was attempted with a fixed possibility ratio. The ratio for making a displacement, rotation, insertion and deletion was set to 4:2:3:3 in GCMC simulation. The initial positions were randomly inserted into the accessible volume of the system. The GCMC simulations were allowed to equilibrate with at least 1×10^8 MC steps before the data production with another 1×10^8 MC steps was run to sample the thermodynamic properties of interest. Details of standard GCMC simulation algorithm can be found elsewhere [48,55].

In a GCMC simulation, the temperature, volume and chemical potential are specified. Thus, from a single GCMC simulation of the adsorbed phase, one can relate the amount adsorbed to the chemical potential of the adsorbed phase. Since, the chemical potential of the adsorbed phase is the same as the bulk phase at equilibrium, this is also the bulk chemical potential. However, in order to generate isotherms in terms of the bulk pressure, we perform a second set of GCMC simulations of the bulk phase at the same set of chemical potentials as used in the adsorbed phase simulations. This allows us to convert the chemical potential to the more practical bulk pressure. Thus, each data point on the isotherm is generated by two simulations, one of the adsorbed phase providing the loading as a function of chemical potential and one of the bulk phase providing the pressure as a function of the same chemical potential. Desbiens et al. [56] have also used a similar procedure to generate each point on the isotherm from distinct simulations of the bulk and adsorbed phase. The two molecular simulation programs (MD and GCMC) have been developed in our laboratory. MD is parallelised using Message Passing Interface (MPI).

4. Results and discussion

4.1 Pure RDX

We performed simulations of RDX in IRMOF-1 at 300 K across a set of loadings that correspond to bulk pressures ranging from 0 (infinite dilution) to 1 bar. In order to obtain good statistical uncertainties, the simulation box representing the adsorbent varies from (12 × 12 × 12) to (325 × 325 × 325) unit cells (as pictured in Figure 1) with the periodic boundary conditions exerted in all three directions. The size of the system is based on obtaining a simulation with a sufficient number of adsorbate molecules (at least 1000), required to obtain reasonable uncertainties. Unless otherwise mentioned, the uncertainties are smaller than the symbol sizes in the figures presented. The resulting adsorption isotherm is shown in Figure 3. The maximum loading studied is less than 0.3 molecules per cage, half of which are big cages and half of which are small cages. We observe from the simulation that at 300 K virtually all RDX molecules are located in big cages. Thus, even at our highest loading we are below 0.6 molecules per big cage. In our simulations we do not observe more than one RDX molecule per cage (either type). We do observe significant nonlinear behaviour in the adsorption isotherm as we begin to have a substantial fraction of the big cages filled with one RDX.

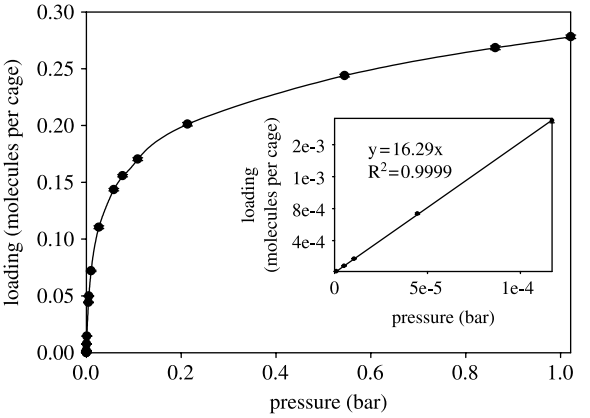

Figure 3. Isotherm of RDX in IRMOF-1 from infinite dilution to 1 bar. The inset shows the linear fitting plot of the infinite dilution data.

At low loadings, we observe the linear part of the isotherm, shown as an insert in Figure 3. This linear regime is particularly of interest because this corresponds to the very low partial pressures of RDX where it is present at realistic ppb or ppt levels. The linear regime extends to about 1×10^{-4} bar, which is well above realistic RDX partial pressures. Thus, all practically relevant systems are in the linear regime. At room temperature, the linear regime is defined by a Henry's law constant of 16.3 molecules/cage bar (21.2 mol/kg/bar) for RDX in IRMOF-1, which is substantially larger than that of hydrogen in IRMOF-1 of 0.3 mol/kg/bar [4], CO_2 in IRMOF-1 of 0.9 mol/kg/bar and CH_4 in IRMOF-1 of 0.4 mol/kg/bar [13].

In Figure 4, we plot isodensity surfaces for the COM of RDX in IRMOF-1 at 300 K and infinite dilution. The volume within these isodensity surfaces is where the highest probability of finding an RDX molecule exists. We will refer to these volumes as adsorption sites. Outside the isodensity surface, a lower RDX density exists. In Figure 4(a)–(c) we show the isodensity surfaces with

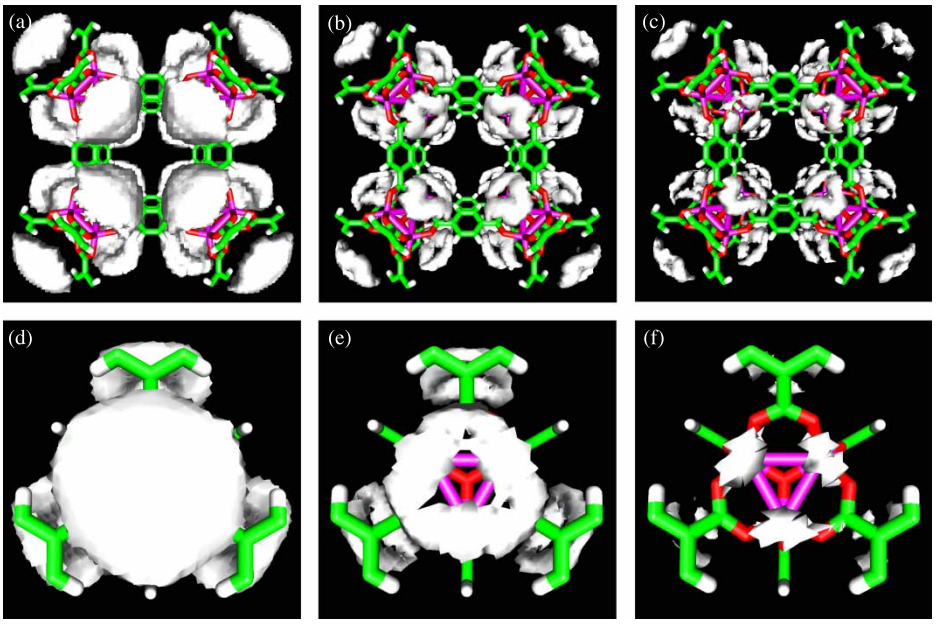

Figure 4. Density distribution of RDX in IRMOF-1 with density contour from low to high (both full cage and vertex view) at 300 K and infinite dilution.

reference to the framework of the entire cage. A small cage is at the centre of the image. All density surfaces are centred around vertices. Each vertex is part of eight cages – four big and four small cages. In Figure 4(a)–(c), the four-fold symmetry of the adsorption sites is readily apparent. These four adsorption sites exist exclusively in the big cages. In other words, all adsorption occurs in the big cages. This is also the case for the adsorption of benzene in IRMOF-1 [57].

In Figure 4(a)–(c), the value of density at which the isodensity surface is plotted is increased from (a) to (c). Thus, the adsorption sites become smaller, defining more localised regions of space with the commensurately higher probabilities of finding RDX molecules. We see that there is an internal structure to the adsorption sites. This internal structure is better visualised by examining Figure 4(d)–(f), in which we show the same isodensity surfaces with reference to a single vertex. In these latter three figures, the viewpoint is from the centre of the big cage. Here, we see that the centre of the adsorption site is not as favourable as an outer ring. Further, increase in the density of the surface shows that there is in fact a three-fold symmetry of sub-sites within the adsorption site. These sub-sites are located between the three benzene rings that extend from the vertex and form the adjacent edges of the big cage. Thus, we can characterise the adsorption of an RDX molecule as (i) residing in a big cage, (ii) near a vertex, and (iii) between benzene rings.

The isodensity surfaces are based on RDX COM positions. For information regarding the orientation of the RDX molecule, we examine snapshots from the simulation. In Figure 5(a) and (b), we show a snapshot of one RDX molecule residing in this adsorption site from the view of the cage and a single vertex. This snapshot was judged to be a typical RDX orientation based on an inspection of a set of snapshots. In this snapshot, we see

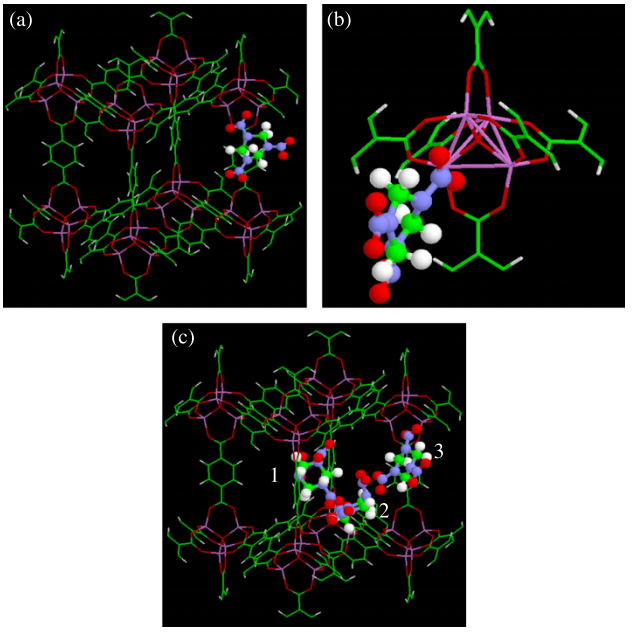

Figure 5. Snapshots of RDX configuration in IRMOF-1 (both full cage and vertex view), RDX is currently residing in one of three adsorption sites around the vertex in a big cage (blue, N; red, O; green, C; white, H).

that there is a strong interaction (Zn–O distance is ~2.0 Å) formed between a Zn atom in the vertex and one of the two O atoms of one of the three nitro groups on the RDX molecule. The second O atom of the same nitro group forms a weaker interaction (Zn–O distance is ~3.6 Å) with another Zn atom in the same vertex. The other two nitro groups are not interacting closely with the vertex. The orientation of the RDX plane (as defined by the three N atoms) is mobile within each sub-site, moving from being nearly parallel with one benzene ring to nearly parallel with the other ring. In Figure 5(c), we show a particular trajectory where an RDX moves from small cage (position 1) to big cage (position 3). This diffusion event can be characterised as a big cage through small cage to big cage motion. However, the RDX molecule ends up at a different vertex. The diffusion event for benzene in IRMOF-1 is also a big cage through small cage to big cage motion, but the molecule is reported to end up at the same vertex [57].

In Figure 6, we show a representative plot of selected structural elements of RDX – the bond distance, bending angles and the torsion – in the ideal gas and in IRMOF-1 at a loading of 0.0625 RDX/cage at 300 K. The solid lines indicate RDX in IRMOF-1 while open symbols represent the bulk gas phase. The RDX molecule undergoes subtle changes in conformation when adsorbed within IRMOF-1

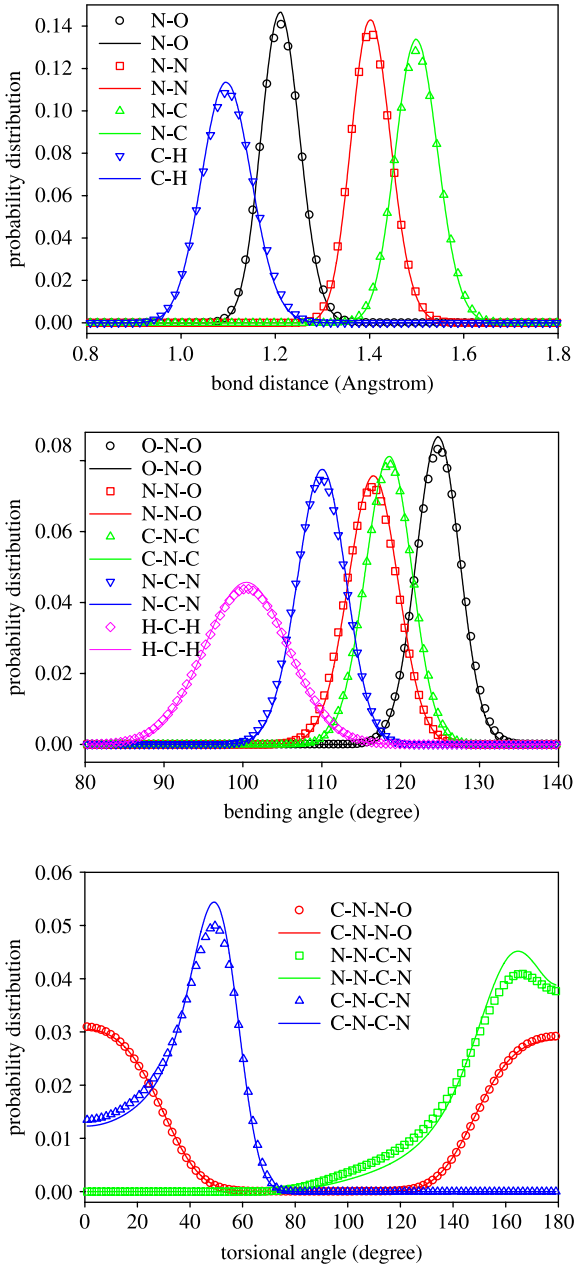

Figure 6. Conformational distribution (bond stretching, bond bending and torsion) in bulk and adsorbed phase at 300 K (properties in bulk phase, open symbols; properties in adsorbed phase, solid lines).

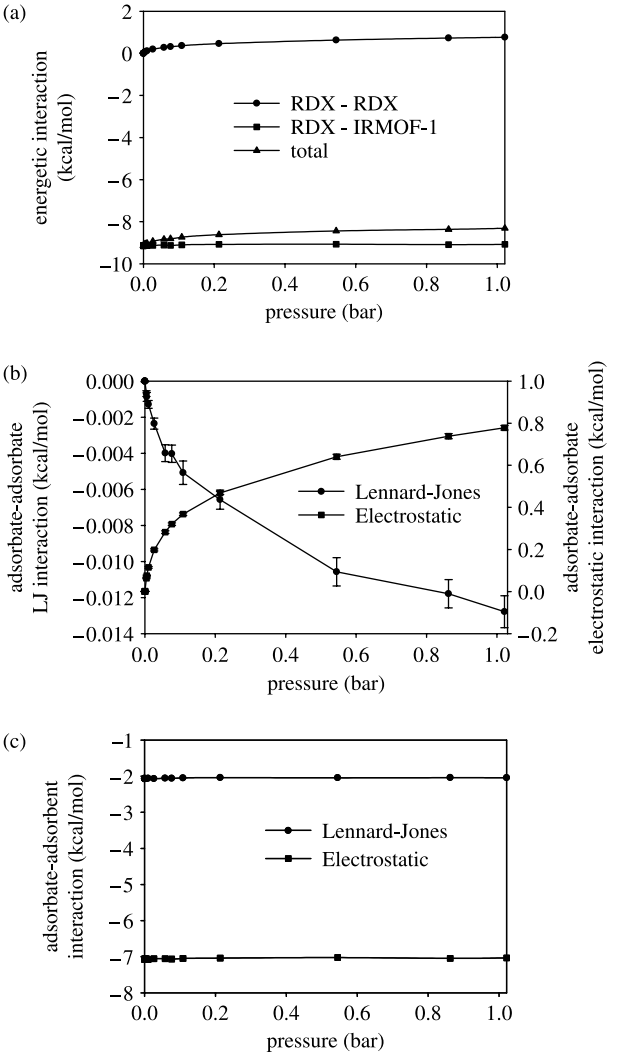

Figure 7. Interaction energies of RDX in IRMOF-1 from infinite dilution to 1 bar at 300 K. The energies are per mole of RDX.

relative to the bulk gas phase at room temperature. In all three plots of Figure 6 we observe that the breadth of the distribution functions for bond distance, bending angles and torsion angles for RDX in IRMOF-1 slightly decreases compared to the bulk but the average values remain the same.

The adsorption energy of RDX in IRMOF-1 at room temperature is shown in Figure 7. As we can see in Figure 7(a), the binding energy is about −9.2 kcal/mol, which is in good agreement with quantum chemistry calculation of −9.8 kcal/mol [58] and −8.8 kcal/mol [59]. The total potential energy in the system increases until 0.2 bar and then changes slightly. We also observe the adsorbate–adsorbate potential energy increases with increasing pressure. This is because of an unfavourable RDX–RDX electrostatic interaction shown in Figure 7(b) and (c), which is likely due to orientations imposed by the framework. The four adsorption sites of RDX have significant attractive electrostatic interactions with the RDX.

In Figure 8, we show self-diffusivities of RDX and average travelled distances at different temperatures, which varie from 200 to 500 K. To determine the self-diffusion coefficient, the mean square displacement (MSD) as shown in Figure 9 is examined. The diffusion regime starts at about 4 ns, with a slope of 1 in the double logarithmic plot of the averaged MSD, shown as an insert in Figure 9. The self-diffusivity of RDX in IRMOF-1 is a strong function of temperature. An Arrhenian fit of the diffusion coefficient $D = D_0 \exp(-E_a/RT)$ is also shown in Figure 8. The activation energy, E_a, for diffusion is 6.0 kcal/mol, which can be compared with activation energy for the diffusion of benzene, methane and ethane in IRMOF-1 of 1.0, 2.0 and 2.3 kcal/mol, respectively [57,60].

In Figure 8, we show the mean distances travelled by the end of the simulation (square root of the final MSD). At 200 K, we do not observe intercage motion, since the average distance travelled is no larger than the cage

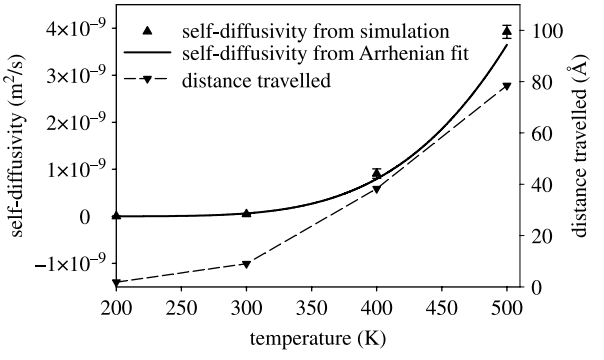

Figure 8. Self-diffusivity and Arrhenian fit for RDX in IRMOF-1, as well as average distance travelled at different temperatures from 200 to 500 K.

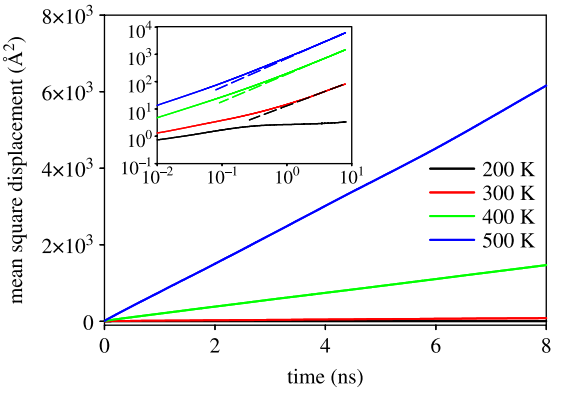

Figure 9. Mean square displacement in different temperatures from 200 to 500 K. The inset shows the log–log plot, giving a slope of 1 (dashed line).

dimension. At room temperature, we find a self diffusivity for RDX in IRMOF-1 of $(4.55 \pm 0.44) \times 10^{-11}$ m²/s, which is two orders of magnitude lower than the diffusion of benzene in IRMOF-1 [57].

For the purposes of preconcentrating RDX for sensors, one naturally wonders if this low RDX diffusivity at room temperature precludes IRMOF-1 as a potential adsorbent based strictly on the mobility critierion. Crystals of IRMOF-1 vary from 50 to 150 μm [61]. Thus, an order of magnitude estimate of the time RDX would take to diffuse out of an IRMOF-1 crystal at room temperature is from 55 to 454 s, which potentially could lie within an operational timescale.

4.2 *RDX in framework with air*

In service as a preconcentrator, the MOF not only adsorbs RDX, but also is struck by other molecules in the air. In our work, we modelled dry air as a mixture of N_2 and O_2. The bulk pressure of the dry air is atmospheric pressure.

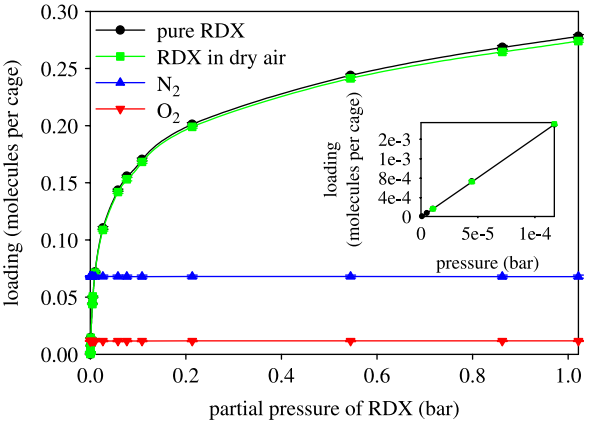

Figure 10. Isotherm of RDX mixed with dry air in IRMOF-1 from infinite dilution to 1 bar. The inset shows the linear fitting plot of the infinite dilution data.

In Figure 10, we show adsorption isotherms for RDX, N_2 and O_2 as a function of the partial pressure of RDX in the bulk phase. This partial pressure of RDX is defined as the product of the mole fraction of RDX and the total pressure in the bulk simulation. In this series of simulations, the chemical potentials of N_2 and O_2 are held constant, while the chemical potential of RDX is varied. We see in Figure 10 that there is very little interaction whatsoever between the three adsorbents. The amount of N_2 and O_2 is virtually independent of the amount of RDX adsorbed. This is because N_2 and O_2 do not have well-defined adsorption sites [62,63] and are present in fairly small quantities. Furthermore, the RDX adsorption isotherm from this mixture is virtually the same as that of pure RDX, especially in the low pressure limit of practical interest (as seen in the insert). The Henry's law constant for RDX in dry air is the same as that for pure RDX isotherm.

We also simulated adsorption of RDX in the presence of wet air. We acknowledged above that in order to quantitatively reproduce adsorption isotherms of water in MOFs, empirical adjustments are required [29,30]. To avoid this empiricism, we performed a series of GCMC simulations of the RDX, N_2 and O_2 in an adsorbent with a fixed number of water molecules. We performed canonical Monte Carlo simulations of the H_2O, translating and rotating them, but not inserting or deleting them. We limit ourselves to low water content, since IRMOF-1 is known to be unstable at higher water contents (>4 wt%) [26].

In Figure 11, we show adsorption isotherms for RDX, N_2 and O_2 at a partial pressure of RDX corresponding to 1 bar as a function of water content in the MOF. We choose a relatively high partial pressure of RDX in order to have a significant amount of RDX present in the system without having to simulate billions of water molecules. The presence of water does not affect the adsorption of N_2 and O_2. However, the amount of RDX adsorbed increases

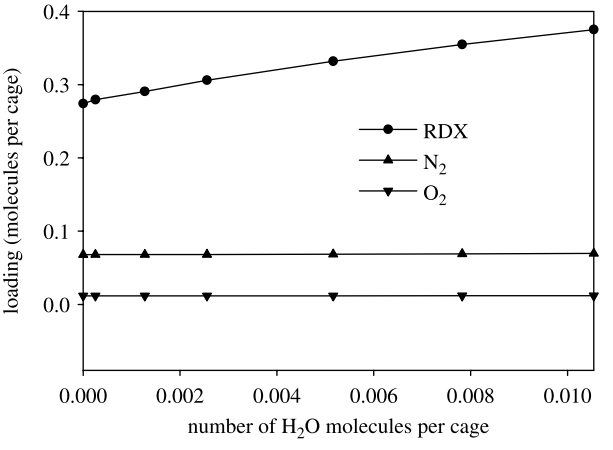

Figure 11. The effect of water on RDX adsorption at 300K. The partial pressure for RDX is 1 bar.

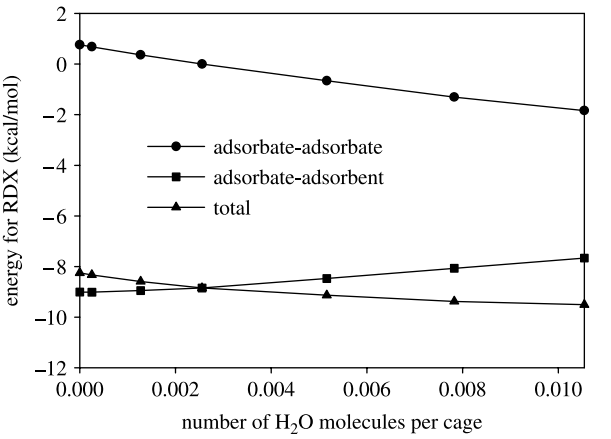

Figure 12. The interaction energies for RDX in mixture (RDX and wet air) at 300 K.

with increasing water content. In order to explain this result, we can examine the contribution to the potential energy as shown in Figure 12. Both water and RDX are competing for adsorption sites near the vertices of the big cage. Therefore, as loading increases, we see an unfavourable increase in the RDX-framework contribution to the potential energy. However, we see a more significant favourable decrease in the interactions between RDX and other adsorbates, due to attractive electrostatic interactions between the water and the RDX. Thus, we see RDX and water molecules clustered around the vertices, paying a slight energetic penalty for sharing adsorption sites that is more than compensated for by the enhanced adsorbate–adsorbate interactions.

5. Conclusions

MD and GCMC simulations have been performed to understand the adsorptive and diffusive behaviour of RDX in IRMOF-1. We generated adsorption isotherms for pure RDX, RDX in dry air, and RDX in wet air. We found a Henry's law constant of 21.2 mol/kg/bar for both pure RDX and RDX in dry air. The presence of water increases the amount of RDX adsorbed. The RDX adsorption sites are located (i) in big cages, (ii) near a vertex, and (iii) between benzene rings. The energy of adsorption of RDX at infinite dilution was found to be -9.2 kcal/mol. The distributions of bond lengths, bond angles and torsion angles in RDX are uniformly slightly broader in the gas phase than in the adsorbed phase, but not markedly so. The self-diffusivity of RDX in IRMOF-1 is a strong function of temperature, with an activation energy of 6.0 kcal/mol. The path for diffusion can be considered as a motion from the deep adsorption site in a big cage through a small cage to another big cage. This path is similar to that shown for benzene in IRMOF-1,

although in that case the destination vertex was the same as the originating vertex, which is not observed for RDX.

Acknowledgements

The authors gratefully acknowledge the financial support of National Science Foundation (NSF) under grant CMMI-0730207. Work at Oak Ridge National Laboratory (ORNL) was supported by the Center for Nanophase Materials Sciences, sponsored by the Division of Scientific User Facilities, U.S. Department of Energy (USDOE) and used resources of the National Center for Computational Sciences (NCCS), ORNL, supported by the Office of Science, USDOE, as well as resources of the National Institute for Computational Sciences (NICS), ORNL, supported by NSF with agreement number: OCI 07-11134.

References

[1] J. Yinon and S. Zitrin, *Modern Methods and Applications in Analysis of Explosives*, Wiley, New York, 1996.
[2] D.S. Moore, *Recent advances in trace explosives detection instrumentation*, Sens. Imaging 8 (2007), pp. 9–38.
[3] M. Eddaoudi, J. Kim, N. Rosi, D. Vodak, J. Wachter, M. O'Keeffe, and O.M. Yaghi, *Systematic design of pore size and functionality in isoreticular MOFs and their application in methane storage*, Science 295 (2002), pp. 469–472.
[4] N.L. Rosi, J. Eckert, M. Eddaoudi, D.T. Vodak, J. Kim, M. O'Keeffe, and O.M. Yaghi, *Hydrogen storage in microporous metal-organic frameworks*, Science 300 (2003), pp. 1127–1129.
[5] J.L.C. Rowsell, A.R. Millward, K.S. Park, and O.M. Yaghi, *Hydrogen sorption in functionalized metal-organic frameworks*, J. Am. Chem. Soc. 126 (2004), pp. 5666–5667.
[6] D.J. Collins and H.C. Zhou, *Hydrogen storage in metal-organic frameworks*, J. Mater. Chem. 17 (2007), pp. 3154–3160.
[7] T. Duren and R.Q. Snurr, *Assessment of isoreticular metal-organic frameworks for adsorption separations: a molecular simulation study of methane/n-butane mixtures*, J. Phys. Chem. B 108 (2004), pp. 15703–15708.
[8] M. Fuentes-Cabrera, D.M. Nicholson, B.G. Sumpter, and M. Widom, *Electronic structure and properties of isoreticular metal-organic frameworks: the case of M-IRMOF1 (M = Zn, Cd, Be, Mg, and Ca)*, J. Chem. Phys. 123 (2005), 124713.
[9] Z. Ni, J.P. Jerrell, K.R. Cadwallader, and R.I. Masel, *Metal-organic frameworks as adsorbents for trapping and preconcentration of organic phosphonates*, Anal. Chem. 79 (2007), pp. 1290–1293.
[10] E.P. Wallis and D.L. Thompson, *Molecular-dynamics simulations of ring inversion in RDX*, J. Chem. Phys. 99 (1993), pp. 2661–2673.
[11] S. Boyd, M. Gravelle, and P. Politzer, *Nonreactive molecular dynamics force field for crystalline hexahydro-1,3,5-trinitro-1,3,5 triazine*, J. Chem. Phys. 124 (2006), 124508.
[12] G. Garberoglio, A.I. Skoulidas, and J.K. Johnson, *Adsorption of gases in metal organic materials: comparison of simulations and experiments*, J. Phys. Chem. B 109 (2005), pp. 13094–13103.
[13] D. Dubbeldam, H. Frost, K.S. Walton, and R.Q. Snurr, *Molecular simulation of adsorption sites of light gases in the metal-organic framework IRMOF-1*, Fluid Phase Equilib. 261 (2007), pp. 152–161.
[14] J.L.C. Rowsell, E.C. Spencer, J. Eckert, J.A.K. Howard, and O.M. Yaghi, *Gas adsorption sites in a large-pore metal-organic framework*, Science 309 (2005), pp. 1350–1354.
[15] B.C. Dionne, D.P. Rounbehler, E.K. Achter, J.R. Hobbs, and D.H. Fine, *Vapor pressure of explosives*, J. Eng. Mater. 4 (1986), pp. 447–472.
[16] C.C. Chambers and D.L. Thompson, *Further-studies of the classical dynamics of the unimolecular dissociation of RDX*, J. Phys. Chem. 99 (1995), pp. 15881–15889.
[17] L.E. Drain, *Permanent electric quadrupole moments of molecules and heats of adsorption*, Trans. Faraday Soc. 49 (1953), pp. 650–654.
[18] J.J. Potoff and J.I. Siepmann, *Vapor–liquid equilibria of mixtures containing alkanes, carbon dioxide, and nitrogen*, AIChE J. 47 (2001), pp. 1676–1682.
[19] L. Zhang and J.I. Siepmann, *Direct calculation of Henry's law constants from Gibbs ensemble Monte Carlo simulations: nitrogen, oxygen, carbon dioxide and methane in ethanol*, Theor. Chem. Acc. 115 (2006), pp. 391–397.
[20] Q.Y. Yang, C.Y. Xue, C.L. Zhong, and J.F. Chen, *Molecular simulation of separation of CO_2 from flue gases in Cu-BTC metal-organic framework*, AIChE J. 53 (2007), pp. 2832–2840.
[21] F. Bresme, J.L.F. Abascal, and E. Lomba, *Theory and simulation of central force model potentials: application to homonuclear diatomic molecules*, J. Chem. Phys. 105 (1996), pp. 10008–10021.
[22] S.D. Bembenek and B.M. Rice, *Transitioning model potentials to real systems. II. Application to molecular oxygen*, J. Chem. Phys. 113 (2000), pp. 2354–2359.
[23] Y.J. Wu, H.L. Tepper, and G.A. Voth, *Flexible simple point-charge water model with improved liquid-state properties*, J. Chem. Phys. 124 (2006), 024503.
[24] W.L. Jorgensen, J.J. Chandrasekhar, J.D. Madura, R.W. Impey, and M.L. Klein, *Comparison of simple potential functions for simulating liquid water*, J. Chem. Phys. 79 (1983), pp. 926–935.
[25] H.J.C. Berendsen, J.P.M. Postma, W.F. van Gunsteren, and J. Hermans, *Interaction models for water in relation to protein hydration*, Intermolecular Forces, Reidel, Dordrecht, Holland, 1981.
[26] J.A. Greathouse and M.D. Allendorf, *The interaction of water with MOF-5 simulated by molecular dynamics*, J. Am. Chem. Soc. 128 (2006), pp. 10678–10679.
[27] O. Teleman, B. Jonsson, and S. Engstrom, *A molecular-dynamics simulation of a water model with intramolecular degrees of freedom*, Mol. Phys. 60 (1987), pp. 193–203.
[28] U.W. Schmitt and G.A. Voth, *The computer simulation of proton transport in water*, J. Chem. Phys. 111 (1999), pp. 9361–9381.
[29] J. Puibasset and R.J.M. Pellenq, *Grand canonical Monte Carlo simulation study of water adsorption in silicalite at 300 K*, J. Phys. Chem. B 112 (2008), pp. 6390–6397.
[30] J.M. Castillo, T.J.H. Vlugt, and S. Calero, *Understanding water adsorption in Cu-BTC metal-organic frameworks*, J. Phys. Chem. C (2008), pp. 15934–15939.
[31] K.T. Thomson, A.V. McCormick, and H.T. Davis, *The effects of a dynamic lattice on methane self-diffusivity calculations in AlPO4-5*, J. Chem. Phys. 112 (2000), pp. 3345–3350.
[32] S. Fritzsche, M. Wolfsberg, R. Haberlandt, P. Demontis, G.B. Suffritti, and A. Tilocca, *About the influence of lattice vibrations on the diffusion of methane in a cation-free LTA zeolite*, Chem. Phys. Lett. 296 (1998), pp. 253–258.
[33] D.I. Kopelevich and H.C. Chang, *Diffusion of inert gases in silica sodalite: importance of lattice flexibility*, J. Chem. Phys. 115 (2001), pp. 9519–9527.
[34] T.J.H. Vlugt and M. Schenk, *Influence of framework flexibility on the adsorption properties of hydrocarbons in the zeolite silicalite*, J. Phys. Chem. B 106 (2002), pp. 12757–12763.
[35] T.R. Forester and W. Smith, *Bluemoon simulations of benzene in silicalite-1 – prediction of free energies and diffusion coefficients*, J. Chem. Soc.-Faraday Trans. 93 (1997), pp. 3249–3257.
[36] S. Jakobtorweihen, M.G. Verbeek, C.P. Lowe, F.J. Keil, and B. Smit, *Understanding the loading dependence of self-diffusion in carbon nanotubes*, Phys. Rev. Lett. 95 (2005), 044501.
[37] A.J. Fletcher, K.M. Thomas, and M.J. Rosseinsky, *Flexibility in metal-organic framework materials: impact on sorption properties*, J. Solid State Chem. 178 (2005), pp. 2491–2510.
[38] R. Babarao and J.W. Jiang, *Molecular screening of metal-organic frameworks for CO_2 storage*, Langmuir 24 (2008), pp. 6270–6278.
[39] H. Frost and R.Q. Snurr, *Design requirements for metal-organic frameworks as hydrogen storage materials*, J. Phys. Chem. C 111 (2007), pp. 18794–18803.
[40] J.C. Liu, J.T. Culp, S. Natesakhawat, B.C. Bockrath, B. Zande, S.G. Sankar, G. Garberoglio, and J.K. Johnson, *Experimental and theoretical studies of gas adsorption in Cu-3(BTC)(2): an effective activation procedure*, J. Phys. Chem. C 111 (2007), pp. 9305–9313.
[41] A.K. Rappé, C.J. Casewit, K.S. Colwell, W.A. Goddard III, and W.M. Skiff, *UFF, a full periodic-table force-field for molecular*

mechanics and molecular-dynamics simulations, J. Am. Chem. Soc. 114 (1992), pp. 10024–10035.
[42] S.L. Mayo, B.D. Olafson, and W.A. Goddard, *Dreiding – a generic force-field for molecular simulations*, J. Phys. Chem. 94 (1990), pp. 8897–8909.
[43] W.L. Jorgensen, D.S. Maxwell, and J. TiradoRives, *Development and testing of the OPLS all-atom force field on conformational energetics and properties of organic liquids*, J. Am. Chem. Soc. 118 (1996), pp. 11225–11236.
[44] J.A. Greathouse and M.D. Allendorf, *Force field validation for molecular dynamics simulations of IRMOF-1 and other isoreticular zinc carboxylate coordination polymers*, J. Phys. Chem. C 112 (2008), pp. 5795–5802.
[45] M. Tafipolsky, S. Amirjalayer, and R. Schmid, Ab initio *parametrized MM3 force field for the metal-organic framework MOF-5*, J. Comput. Chem. 28 (2007), pp. 1169–1176.
[46] N.L. Allinger, Y.H. Yuh, and J.H. Lii, *Molecular mechanics – the Mm3 force-field for hydrocarbons.1*, J. Am. Chem. Soc. 111 (1989), pp. 8551–8566.
[47] N.L. Allinger, X.F. Zhou, and J. Bergsma, *Molecular mechanics parameters*, Theochem-J. Mol. Struct. 118 (1994), pp. 69–83.
[48] M.P. Allen and D.J. Tildesley, *Computer Simulation of Liquids*, Oxford Science Publications, Oxford, 1987.
[49] D. Wolf, P. Keblinski, S.R. Phillpot, and J. Eggebrecht, *Exact method for the simulation of Coulombic systems by spherically truncated, pairwise r^{-1} summation*, J. Chem. Phys. 110 (1999), pp. 8254–8282.
[50] M. Tuckerman, B.J. Berne, and G.J. Martyna, *Reversible multiple time scale molecular-dynamics*, J. Chem. Phys. 97 (1992), pp. 1990–2001.
[51] S. Nose, *A molecular-dynamics method for simulations in the canonical ensemble*, Mol. Phys. 52 (1984), pp. 255–268.
[52] W.G. Hoover, *Canonical dynamics – equilibrium phase-space distributions*, Phys. Rev. A 31 (1985), pp. 1695–1697.
[53] Q.Y. Wang, J.K. Johnson, and J.Q. Broughton, *Path integral grand canonical Monte Carlo*, J. Chem. Phys. 107 (1997), pp. 5108–5117.
[54] N. Metropolis, A.W. Rosenbluth, M.N. Rosenbluth, A.H. Teller, and E. Teller, *Equation of state calculations by fast computing machines*, J. Chem. Phys. 21 (1953), pp. 1087–1092.
[55] D. Frenkel and B. Smit, *Understanding Molecular Simulation: From Algorithms to Applications*, Academic Press, San Diego, CA, 1996.
[56] N. Desbiens, A. Boutin, and I. Demachy, *Water condensation in hydrophobic silicalite-1 zeolite: a molecular simulation study*, J. Phys. Chem. B 109 (2005), pp. 24071–24076.
[57] S. Amirjalayer, M. Tafipolsky, and R. Schmid, *Molecular dynamics simulation of benzene diffusion in MOF-5: importance of lattice dynamics*, Angew. Chem.-Int. Ed. 46 (2007), pp. 463–466.
[58] J. Leszczynski, T. Petrova, and A. Michalkova, *Theoretical Study of RDX and TATP Interactions with MOF-5*, Physical Science and Technology Conference, 2008.
[59] T. Petrova, A. Michalkova, and J. Leszczynski, *Adsorption of RDX and TATP on MOF-5 – An* ab initio study, J. Phys. Chem. C (under review).
[60] F. Stallmach, S. Groger, V. Kunzel, J. Karger, O.M. Yaghi, M. Hesse, and U. Muller, *NMR studies on the diffusion of hydrocarbons on the metal-organic framework material MOF-5*, Angew. Chem.-Int. Ed. 45 (2006), pp. 2123–2126.
[61] U. Mueller, M. Schubert, F. Teich, H. Puetter, K. Schierle-Arndt, and J. Pastre, *Metal-organic frameworks – prospective industrial applications*, J. Mater. Chem. 16 (2006), pp. 626–636.
[62] K.S. Walton and R.Q. Snurr, *Applicability of the BET method for determining surface areas of microporous metal-organic frameworks*, J. Am. Chem. Soc. 129 (2007), pp. 8552–8556.
[63] E. Garcia-Perez, J. Gascon, V. Morales-Florez, J.M. Castillo, F. Kapteijn, and S. Calero, *Identification of adsorption sites in Cu-BTC by experimentation and molecular simulation*, Langmuir 25 (2009), pp. 1725–1731.